Vibronic Transitions and Quantum Dynamics in Molecular Oligomers: A Theoretical Analysis with an Application to Aggregates of Perylene Bisimides

J. Seibt,[†] T. Winkler,[†] K. Renziehausen,[†] V. Dehm,[‡] F. Würthner,[‡] H.-D. Meyer,[§] and V. Engel*,[†]

Institut für Physikalische Chemie and Institut für Organische Chemie, Universität Würzburg Am Hubland, D-97074 Würzburg, Germany, and Theoretische Chemie, Universität Heidelberg, Im Neuenheimer Feld 229, D-69120 Heidelberg, Germany

Received: May 26, 2009; Revised Manuscript Received: September 15, 2009

Vibronic absorption spectra of molecular aggregates consisting of up to $N = 9$ monomer units are calculated employing methods of time-dependent quantum mechanics. Taking one vibrational degree of freedom for each monomer into account and treating one-exciton excited electronic states leads to a problem with N vibrations and N electronically coupled states. The demanding quantum propagation is carried out within the multiconfiguration time-depended Hartree method (MCTDH). Spectral features of and population transfer in the aggregates are analyzed as a function of the aggregate size and the strength of the electronic coupling. With a model for oligomers of perylene bisimides, it is shown how measured temperature-dependent absorption spectra correlate with the aggregate size. Furthermore, the exciton localization and dynamics in these aggregates are investigated.

1. Introduction

UV−vis spectra of smaller molecular aggregates usually exhibit an electronic band structure with—in many cases—a superimposed vibrational fine-structure. As a consequence, a theoretical characterization of the absorption (and likewise emission) properties of such systems needs the inclusion of vibrational degrees of freedom in the respective Hamiltonians. This was realized very early,[1] but it took some time until the advances in computer technology allowed for numerical calculations of absorption spectra. A first numerical study was presented by Fulton and Gouterman[2] on a molecular dimer. Since then, many theoretical studies of dimer systems including vibrations have been performed; see, e.g., refs 3−12.Employing the same vibronic models, numerically exact studies on trimers and larger aggregates[13−15] were performed. However, these approaches using basis set or grid methods are limited due to restricted computer power. It would, however, be highly desirable to be able to systematically increase the number of aggregated monomers and to monitor the changes in the respective spectra. Although this is possible employing approximate schemes like the Coherent Exciton Scattering approximation by Briggs and Herzenberg[16,11,17] or the Two Particle Approximation,[18−20] it is worthwhile to tackle such problems with schemes to solve the Schrödinger equation numerically exact without employing further approximations.

Regard, as an example, our recent experiments on the aggregation of perylene bisimide dyes.[21,22] In this earlier work we have investigated the formation of extended aggregates in solution and the organization in liquid-crystalline mesophases that exhibit excimer-type emission properties and pronounced charge-carrier mobility along the columnar π -stack. Systematic changes of UV−vis spectra upon changes of concentration and also temperature suggested a one-dimensional aggregation process leading to columnar π-stacks.[21,22] For general reviews on perylene bisimides (PBI), see refs 23−25. In performing an analysis of our temperature-dependent spectra,[22] we were able to deduce the distributions of aggregates present at specific temperatures. This analysis rested on a classical aggregation model, and in the present work we attempt to give further evidence of the distributions in calculating the UV−vis spectra of different oligomers employing methods of time-dependent quantum mechanics. As mentioned above, therefore, an efficient propagation method is mandatory. Fortunately, with the multiconfiguration time-dependent Hartree (MCTDH) method,[26−30] a technique is now available to treat systems with a larger number of degrees of freedom. We employ this method for the calculation of the spectra and are thus able to compare the results to experiment.

As a second aspect, the quantum dynamics in the oligomers is investigated. This is connected to the question of electronic energy transfer (or exciton transfer) in molecular aggregates[31] which was addressed already in the early work of Franck and Teller[32] or Merrifield.[33] Recently, the aspect of the influence of vibronic coupling on the energy transfer was discussed extensively by Roden et al.[34] Here, we concentrate on the general features of the dynamics depending on the electronic coupling strength and aggregates size and also on the role of the exciton localization in the PBI-aggregates. The paper is organized as follows: in section 2 we summarize the theoretical methods employed for the calculation of the spectra and outline the aggregate model. The results are presented in section 3 which include the comparison to experiment. A summary is then given in section 4.

2. Theory and Model

2.1. Absorption Spectra. We calculate absorption spectra for electronic transitions employing wave packet propagation techniques.[35−38] Within a time-dependent approach, the spectrum is given as

* Corresponding author: phone, +49-931-318-6376; fax, +49-931-888-6362; e-mail, voen@phys-chemie.uni-wuerzburg.de.
[†] Institut für Physikalische Chemie, Universität Würzburg, Am Hubland.
[‡] Institut für Organische Chemie, Universität Würzburg, Am Hubland.
[§] Theoretische Chemie, Universität Heidelberg, Im Neuenheimer Feld.

10.1021/jp904892v CCC: $40.75
Published on Web 10/15/2009

$$\sigma_i(E_{\mathrm{ph}}) \sim \int \mathrm{d}t\, \mathrm{e}^{i(E_i+E_{\mathrm{ph}})t/\hbar} c_i(t) w(t) \tag{1}$$

with the photon energy E_{ph} and the time-correlation function:

$$c_{\mathrm{i}}(t) = \langle \vec{\varepsilon}\,\vec{\mu}\psi_{\mathrm{i}} | e^{-iH_{\mathrm{e}}t/\hbar} | \vec{\varepsilon}\,\vec{\mu}\psi_{\mathrm{i}} \rangle \tag{2}$$

Here $\vec{\mu}$ is the transition dipole operator and $\vec{\varepsilon}$ is the electric field polarization vector. The initial state (vibrational state in the electronic ground state) of energy E_{i} is denoted as ψ_{i}, and H_{e} is the Hamiltonian of the excited state. Additionally, the Fourier transform in eq 1 contains a window function $w(t)$ which damps the correlation function at longer time giving rise to a spectral broadening.[39] In our numerical calculations we employ a Gaussian form for $w(t)$ having a width (full width at half-maximum) of Δ_t which then results in an energy resolution of $\Delta E_{\mathrm{res}} = 8\ \ln(2)\hbar/\Delta_{\mathrm{t}}$.

2.2. Model Hamiltonian. In our treatment, a monomer (M) is described within a model consisting of the ground ($|g\rangle$), and an excited electronic state ($|e\rangle$) so that the Hamiltonian reads

$$H^{\mathrm{M}}(x) = |g\rangle H_{\mathrm{g}}(x)\langle g| \ + \ |e\rangle H_{\mathrm{e}}(x)\langle e| \tag{3}$$

where x is a (scaled) vibrational coordinate. The vibrational Hamiltonians are

$$H_{\mathrm{g}}(x) = -\frac{1}{2}\frac{\mathrm{d}^2}{\mathrm{d}x^2} + \frac{1}{2}\omega^2 x^2 \tag{4}$$

$$H_{\mathrm{e}}(x) = -\frac{1}{2}\frac{\mathrm{d}^2}{\mathrm{d}x^2} + \frac{1}{2}\omega^2 (x - x_{\mathrm{e}})^2 + \Delta E \tag{5}$$

Thus, we use two harmonic oscillators with equal frequency ω which are shifted in energy (ΔE) and in their equilibrium distance (x_{e}).

The Hamiltonian for an oligomer consisting of N monomers is constructed from the monomer model as follows. Because of the weak (van der Waals) interaction between the monomers in their electronic ground state, the respective Hamiltonian is approximated as separable

$$H_{\mathrm{g}}{}^{N}(\vec{x}) = H_{\mathrm{g}}{}^{N}(x_1, x_2, ..., x_N) = \sum_{n=1}^{N} |g\rangle H_{\mathrm{g}}(x_n)\langle g| \tag{6}$$

where x_n denotes the internal coordinate of monomer (n) and we used the abbreviation

$$|g\rangle = |g(1), g(2), ..., g(N)\rangle \tag{7}$$

The excited electronic states are described within the one-exciton approximation neglecting exchange effects.[40] This means that one considers N degenerate configurations which correspond to the excitation of a single monomer within the aggregate. The respective electronic states are

$$|n\rangle = |g(1), ..., g(n-1), e(n), g(n+1), ..., g(N)\rangle \tag{8}$$

These states are coupled by electronic coupling elements J. Regarding only next neighbor interactions, the excited state Hamiltonian takes the form

$$H_{\mathrm{e}}{}^{N}(\vec{x}) = \sum_{n=1}^{N} |n\rangle H_{\mathrm{e},n}(\vec{x})\langle n| \ + \sum_{n=1}^{N-1} |n\rangle J\langle n+1| \ + \sum_{n=1}^{N-1} |n+1\rangle J\langle n| \tag{9}$$

where we have set all coupling elements equal. Furthermore, these elements will be treated as coordinate independent, i.e., J enters as a single coupling-strength parameter. The vibrational Hamiltonians are of the form

$$H_{\mathrm{e},n}(\vec{x}) = H_{\mathrm{e}}(x_n) + \sum_{(m\neq n)=1}^{N} H_{\mathrm{g}}(x_m) \tag{10}$$

We note that an identical energy shift ΔE for all oligomers is used, whereas, in general, these shifts are size-dependent. Disorder effects are not included here.[41,19,42,20,43] The role of charge-transfer states in PBI aggregates is not fully understood. In our recent quantum chemical study of perylene bisimide dimers[44] it was shown that the inclusion of the neutral states can fully account for the absorption and emission properties of the dimers; see also the discussion in ref 45. Therefore we restrict our model to the neutral manifold of electronic states. The excited state Hamiltonian describes a system with N internal degrees of freedom and N coupled electronic states. The operator $H_{\mathrm{e},n}$ can be regarded as belonging to a *diabatic state* because it is coupled to other states via a potential coupling matrix element.

The absorption spectra strongly depend on the orientation of the transition dipole moments $\vec{\mu}_n$ of the single monomers (n) which build the aggregate. These vectors are assumed to lie in a plane and the angles γ between dipole moments of neighboring monomers are taken as equal. The dipole vector of monomer (n) is

$$\vec{\mu_n} = \mu_n(\cos[\varphi + (n-1)\gamma]\sin[\Theta], \sin[\varphi + (n-1)\gamma]\sin[\Theta], \cos[\Theta]) \tag{11}$$

Choosing the field polarization vector as $\vec{\varepsilon} = (1/2^{1/2})(1, 1, 0)$ and evaluating the scalar product

$$\vec{\varepsilon}\,\vec{\mu} \ = \ \sum_{n=1}^{N} \vec{\varepsilon}\,\vec{\mu}_n \tag{12}$$

yields the correlation function

$$c_{\mathrm{i}}(\varphi, \Theta, \gamma, t) = \frac{1}{2}\sum_{n=1}^{N}\sum_{m=1}^{N} \langle \mu_n\psi_i | \mathrm{e}^{-iH_{\mathrm{e}}{}^{N}t/\hbar} | \mu_m\psi_i \rangle f_{nm}(\varphi, \Theta, \gamma) \tag{13}$$

with the angular dependent functions

$$f_{nm}(\varphi, \Theta, \gamma) = \sin^2(\Theta)(\cos[(n-m)\gamma] + \sin[2\varphi + (n + m - 2)\gamma]) \tag{14}$$

The average of these functions over all orientations yields the correlation function

$$c_i(\gamma, t) = \left(\frac{1}{3}\right)\sum_{n=1}^{N}\sum_{m=1}^{N}\langle\mu_n\psi_i|e^{-iH_e^N t/\hbar}|\mu_m\psi_i\rangle\cos[(n-m)\gamma] \quad (15)$$

Note that the excited state Hamiltonian H_e^N is a matrix of dimension $N \times N$ and that the vibrational wave function consists of N components. The state vector $|\mu_m\psi_i\rangle$ appearing in the scalar product in eq 13 is

$$|\mu_m\psi_i\rangle = (0, \ldots 0, \mu\psi_i, 0, \ldots 0) \quad (16)$$

so that its mth component contains the product of the monomer (m) transition dipole moment ($|\vec{\mu}_m| = \mu$) and the initial function ψ_i, whereas all other components are equal to zero.

In the numerical calculation, we employ parameters which were determined from our studies of the optical properties of perylene bisimide aggregates.[12] The values for the oscillator frequency and the energy shift are $\omega = 0.175$ eV and $\Delta E = 2.35$ eV. The equilibrium distance in the excited state is $x_e = 2.57$ eV$^{-1/2}$, and the transition dipole moments are chosen within the Condon approximation as a constant. The values of the vibrational shift x_e and the frequency ω correspond to a Huang−Rhys factor of 0.76, which is the important (dimensionless) parameter that determines the intensity of the vibrational transitions. The different choices for the coupling J and the orientation angle γ will be specified below.

2.3. MCTDH. The calculation of the correlation function (and thus the absorption spectrum) requires the propagation of wave packets in the coupled excited electronic states. For larger oligomers, this is a computational challenge. Direct grid methods cannot handle the numerical effort, and therefore we employ the Heidelberg package[46] of the multiconfiguration time-dependent Hartree (MCTDH) method.[26−30]

The MCTDH method achieves its efficiency through a very compact form of the wave function. The MCTDH *ansatz* for the wave function reads

$$\Psi(x_1, \ldots, x_f, t) = \sum_{j_1=1}^{n_1}\ldots\sum_{j_f=1}^{n_f}A_{j_1\ldots j_f}(t)\prod_{\kappa=1}^{f}\varphi_{j_\kappa}^{(\kappa)}(x_\kappa, t) \quad (17)$$

where $x_1, \ldots, x_f$ are the nuclear coordinates, the $A_{j_1\ldots j_f}$ denote the MCTDH expansion coefficients, and the $\varphi_{j_\kappa}^{(\kappa)}$ are the n_κ expansion functions for each degree of freedom κ, known as *single-particle functions* (SPFs). There are f (nuclear) degrees of freedom. Electronic states are treated in the so-called *multiset* formulation, i.e., the wave function is written as a vector, the components of which refer to the electronic states. Each component wave function is of MCTDH form, eq 17. Remember that for the present investigation the number of electronic states as well as the number of degrees of freedom, f, equals the number of monomers, N. The total wave function then is

$$(\psi_1(x_1, \ldots, x_N, t), \psi_2(x_1, \ldots, x_N, t), \ldots, \psi_N(x_1, \ldots, x_N, t))^T \quad (18)$$

The single-particle functions are given only numerically, the MCTDH algorithm provides equations of motion for them. To represent them, an underlying primitive basis, usually a DVR (discrete variable representation[47]) grid, is used. In an actual calculation one has to ensure the convergence of the SPFs with respect to the primitive basis and the convergence of the total wave function with respect to the SPFs. The number of SPFs needed for convergence, n_κ, is usually much smaller than the number of grid points. This is what makes MCTDH efficient. In our numerical calculation a grid ranging from −15.3 eV$^{-1/2}$ to 15.3 eV$^{-1/2}$ with 40 grid points in each coordinate is employed, and a choice of four SPFs in each vibrational degree of freedom proved to be sufficient to achieve convergence.

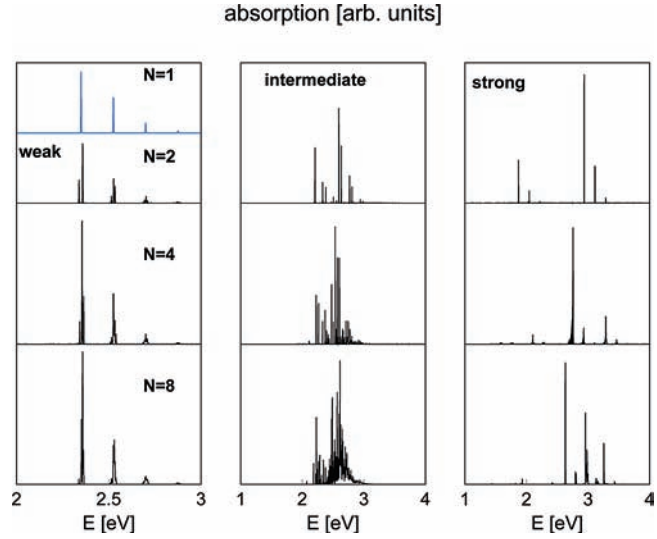

Figure 1. Vibronic absorption spectra of aggregates with different sizes N, as indicated. The left, middle, and right panels contain curves for electronic coupling elements of $J = 0.0175$ eV (weak), $J = 0.175$ eV (intermediate), and $J = 0.525$ eV (strong) coupling, respectively.

3. Results

3.1. Absorption Spectra. Let us first discuss features of the vibronic absorption spectra of the oligomers. Therefore, we regard cases with three different coupling strengths J. They are referred to as weak ($J = 0.0175$ eV), intermediate ($J = 0.175$ eV), and strong ($J = 0.525$ eV) couplings, respectively. This classification is taken in comparing the vibrational monomer spacing ($\omega = 0.175$ eV) with the value of the electronic coupling. We note that this division is consistent to the one given by Simpson and Peterson.[48] The Simpson−Peterson parameter is the ratio between the exciton bandwidth ($2J$) and the monomer bandwidth which amounts to 2ω, in our case. This can be seen in the upper left panel of Figure 1, which shows the monomer spectrum. Weak/strong coupling means that J/ω assumes values essentially smaller/larger than 1. In Figure 1, spectra calculated for these couplings and different aggregate sizes are depicted, as indicated. The energy resolution is taken as $\Delta E_{res} = 0.0024$ eV, and the orientation angle is fixed to $\gamma = 60°$. The monomer spectrum exhibits a vibrational progression with a most intense first peak ((0−0)). This feature remains with increasing aggregate size. We note, that there are cases where the ratio of the first and second vibrational band ((0−0)/(0−1) transitions) is inverted, as has been carefully analyzed by Spano[49] and has been applied for the interpretation of measured polymer spectra.[50,51] In our case this does not happen because the Huang−Rhys factor has a value of $S = 0.76$, whereas it should assume a value of about $S = 1$ to show the inversion. Furthermore, the ratio of the coupling strength and the vibrational frequency is 1/10 in our (weak coupling) case which is also unfavorable to observe the mentioned changes in the peak intensity; see the discussion in ref 49.

Regarding the case of small coupling first, the dimer spectrum resembles very much the monomer spectrum. There, a vibrational progression is present with three lines characterizing transitions with non-negligible Franck−Condon factors. In the dimer, however, one finds a fine-structure in the vibrational bands. For example, the one appearing at the smallest energy splits into two lines. For the larger aggregates ($N = 4, 8$) one observes a splitting of the low energy band into four and eight lines, respectively. An analysis of the other bands at higher energies leads to an even more complex level structure.

To understand the principle of the splitting, it is sufficient to discuss the dimer case in a restricted space of states. Therefore we regard monomer configurations with wave functions

$$\psi_0(x_1, x_2) = \varphi_0^{\mathrm{e}}(x_1)\varphi_0^{\mathrm{g}}(x_2) \tag{19}$$

$$\psi_1(x_1, x_2) = \varphi_1^{\mathrm{e}}(x_1)\varphi_0^{\mathrm{g}}(x_2) \tag{20}$$

$$\tilde{\psi}_0(x_1, x_2) = \varphi_0^{\mathrm{g}}(x_1)\varphi_0^{\mathrm{e}}(x_2) \tag{21}$$

$$\tilde{\psi}_1(x_1, x_2) = \varphi_0^{\mathrm{g}}(x_1)\varphi_1^{\mathrm{e}}(x_2) \tag{22}$$

with energies E_0 (for $\psi_0, \tilde{\psi}_0$) and E_1 (for $\psi_1, \tilde{\psi}_1$). Here, for example, ψ_0 corresponds to the situation where monomer (1) is in its vibrational ground state in the electronic excited state and monomer (2) is in the vibrational ground state in the electronic ground state, etc. This leads to the (restricted) dimer Hamiltonian

$$\mathbf{H}_{\mathrm{e}} = \begin{pmatrix} E_0 & 0 & J_{00} & J_{01} \\ 0 & E_1 & J_{10} & J_{11} \\ J_{00} & J_{10} & E_0 & 0 \\ J_{01} & J_{11} & 0 & E_1 \end{pmatrix} \tag{23}$$

The off-diagonal elements are a product of the electronic coupling parameter J and Franck−Condon factors

$$J_{nm} = J\langle\psi_n|\tilde{\psi}_m\rangle \tag{24}$$

If we neglect the couplings between states of different vibrational energy, i.e., set $J_{01} = J_{10} = 0$, diagonalization of the Hamiltonian eq 23 yields the eigenvalues $\lambda_0^{\pm} = E_0 \pm J_{00}$ and $\lambda_1^{\pm} = E_1 \pm J_{11}$. Thus, each monomer vibrational level is split into two as was discussed above.

The picture just mentioned breaks down if the vibrational level spacing becomes comparable to the electronic coupling which is the case of intermediate coupling. The spectra then exhibit a complicated vibrational structure with a high density of states and there is no simple way to identify the origin of the energy levels.

Despite the complex spectral features encountered for intermediate couplings, the spectra appear more regular in the case $\omega \ll J$, so that for the dimer, two electronic bands appear which are well separated and exhibit a vibrational fine-structure. It is, however, not possible to develop a simple approximate picture for the spectral features as in the case of weak coupling. The $N = 4$ aggregate shows four vibronic bands. Increasing the aggregate size to $N = 8$ results in a spectrum with overlapping vibronic bands so that, again, a very complex line structure is encountered. It has to be noted that, under conditions where aggregates build in solution, it is unlikely that finer details of a vibrational structure are seen in a measured absorption spectrum. We discuss features of such low resolution spectra in connection with experiments on perylene bisimide dyes in section 3.3.

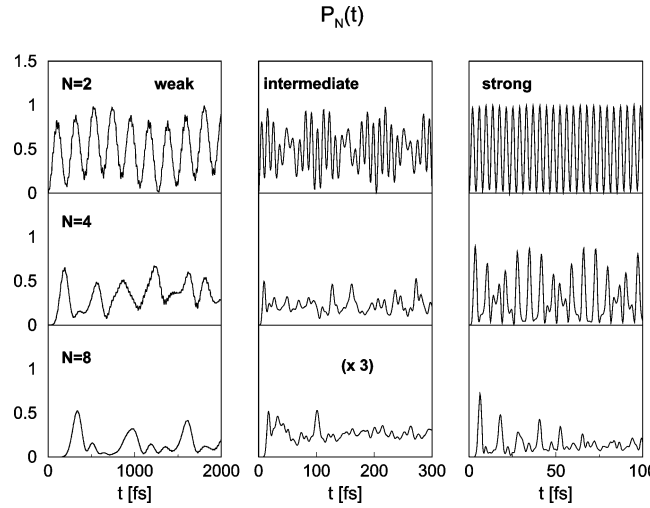

Figure 2. Population dynamics corresponding to the couplings and aggregate sizes as regarded in Figure 1. Shown are the populations $P_N(t)$ corresponding to the excited state where the last monomer N is excited. Because initially only the configuration with monomer $n = 1$ is populated, the curves exhibit the population dynamics from one to the other end of the aggregate.

3.2. Population Dynamics. The different (diabatic) electronic states in our model correspond to configurations where one monomer in the aggregate carries the electronic excitation energy. If the energy is localized in monomer (j) with configuration ($M_1 - M_2 - ... - M_{j-1} - M_j^* - M_{j+1} - ... - M_N$), it is transferred within the aggregate which is commonly called an exciton transfer.[40,52] We now discuss the quantum dynamics of such a transfer for the three coupling cases and aggregates sizes treated in section 3.1. As a measure we take the population dynamics which goes in hand with the energy transfer.[53] In more detail, we regard the case that at time $t = 0$, only the first monomer in the aggregate is excited, i.e., the initial state for the excited state time-propagation is

$$(\psi_1(0), \psi_2(0), ..., \psi_N(0)) = (\mu_1\psi_i, 0, 0, ..., 0) \tag{25}$$

Then, the population which measures the excitation of monomer N is calculated as

$$P_N(t) = \langle\psi_N(t)|\psi_N(t)\rangle \tag{26}$$

This function reflects the time and the efficiency of the energy transfer from one to the other end of the aggregate. Below, the time it takes for $P_N(t)$ to assume its first maximum is called the transfer time t_{tr}.

Figure 2 shows the population dynamics for the various cases, as indicated. Note the different time scales in the three examples. In the weak coupling case, and for the dimer, one finds an oscillating curve where it takes about 110 fs for the energy transfer. This time correlates with the vibrational sublevel splitting. For example, taking the first two lines of the dimer spectrum resulting from the excited state ground vibrational level splitting one calculates a time of 220 fs for the vibrational period which matches the result of the numerical calculation. A closer inspection of the curve shows that there is a faster oscillation

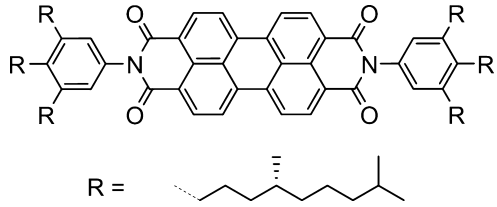

Figure 3. Structure of recently investigated PBI dye.

with smaller amplitude which occurs with about 20 fs. This oscillation period can be connected to the separation of the neighboring vibrational bands.

As expected, with increasing aggregate size, it takes longer for the population transfer. This is consistent with the smaller energy splitting in the vibrational bands. We find transfer times of of $t_{tr} = 187$ fs ($N = 4$) and $t = 340$ fs ($N = 8$) for the first maximum to occur in $P_N(t)$. Because of the increasing level complexity with increasing aggregate size, the population curves become more and more complicated and—at least on the time-scale shown—no clear periodicities can be detected. Also, the efficiency of the transfer diminishes for the larger aggregates. For example, in the $N = 8$ case, only 50% of the population reaches the end of the aggregate during the first period.

If the coupling is increased (intermediate coupling), it takes less time for the population/energy transfer. We find transfer times of 5.5, 9.5, and 17.25 fs for the dimer, tetramer, and octamer, respectively. For the dimer, a clear structure in the time-dependent population curve is found. It consists of a beating pattern which can be traced back to the sum and difference frequencies of the vibrational and electronic frequencies. They belong to values of $T_{vib} = 23.4$ fs and $T_J = 11.7$ fs, giving rise to periods of $T_+ = 15.6$ fs (sum) and $T_- = 46.8$ fs (difference). With increasing number of bound monomers this simple decomposition is no longer possible. Also, in the $N = 8$ case, only about 12% of the population is transferred to the end of the aggregate chain, in the average. This value suggests a (time-independent) equal average population of all excited state configurations.

As we found in the case of the absorption spectra, the strong coupling case is easier to interpret than the one for intermediate coupling. The dimer function shows as strictly periodic behavior with a period given by $\hbar\pi/J = 4$ fs, so that the transfer time is 2 fs. Increasing the aggregate size leads to curves which exhibit longer transfer times of $t_{tr} = 3.5$ and 6.5 fs for the case of $N = 4$, 8, respectively. Because of dispersion, the transfer time is increased while the efficiency (at t_{tr}) diminishes by a factor of 1.3 comparing the dimer and octamer.

To summarize the trends that can be taken from Figure 2, the exciton transfer in the dimer is efficient, is independent of the coupling strength, and can be maintained for a long time (in our model which excludes dissipation effects). For larger oligomers, the transfer efficiency decreases and is smallest for an intermediate coupling.

3.3. Comparison to Experiment. In section 3.1 we discussed features of calculated vibrationally resolved absorption spectra for several coupling strengths and aggregate sizes. In what follows, we demonstrate that such model studies can prove to be important for the interpretation of experiments performed under different conditions.

Recently, we have characterized absorption properties of aggregates of perylene bisimides (PBI). The structure of the monomer is depicted in Figure 3. In Figure 4, we show absorption spectra of aggregates of PBI taken at different temperatures. The temperature-dependent UV−vis spectra of

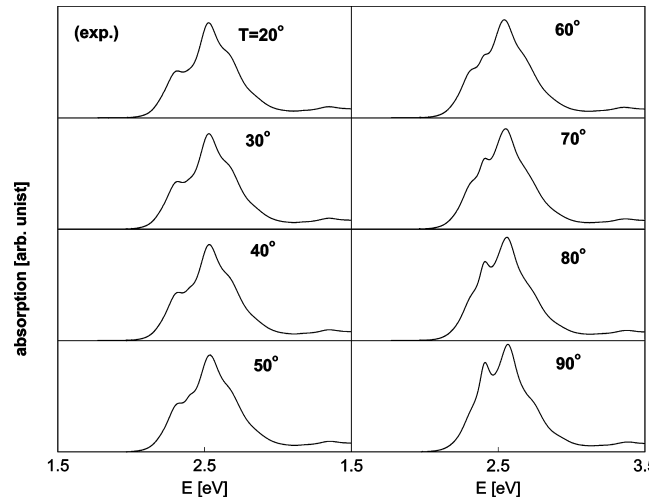

Figure 4. Measured absorption spectra of a 2×10^{-3} M solution of the PBI dye in methylcyclohexane. The spectra were taken at different temperatures (in ° C), as indicated.

the PBI in methylcyclohexane (MCH) have been published previously.[22] They were measured on a Perkin-Elmer Lambda 40P spectrophotometer equipped with a Peltier System as temperature controller and spectroscopic grade solvents were used. A 2×10^{-3} M solution of the PBI in MCH was employed with a 0.1 mm quartz glass cell, for further details consult ref 22.

The spectrum at 90 °C exhibits two main bands of different intensities at energies of $E_1 = 2.41$ eV and $E_2 = 2.57$ eV, respectively. In going from higher ($T = 90$ °C) to lower temperature ($T = 20$ °C) the band maxima shift to smaller energies ($E_1 = 2.31$ eV, $E_2 = 2.52$ eV). However, the most significant change is the value for the relative band intensity. The latter changes monotonically as a function of temperature. Whereas at the lowest temperature a value of $\sigma(E_2)/\sigma(E_1) \sim 2$ is obtained, two bands of almost equal intensities are found at $T = 90$ °C.

It is reasonable to assume that at low temperature larger aggregates exist while, upon heating, they dissociate and only smaller oligomers remain. In our former work,[22] we determined the average aggregation number by UV−vis spectroscopy for different temperatures employing the isodesmic model that assumes equal binding constants for subsequent binding events of a growing π-stack.[54] This led to average aggregation numbers of $N = 2$ ($T = 90$ °C), $N = 2$ ($T = 80$ °C), $N = 3$ ($T = 70$ °C), $N = 4$ ($T = 60$ °C), $N = 5$ ($T = 50$ °C), $N = 6$ ($T = 40$ °C), $N = 8$ ($T = 60$ °C), and $N = 13$ ($T = 20$ °C), respectively. These results were in very good agreement with our earlier investigations with DOSY-NMR and vapor pressure osmometry.[21]

In what follows, we show that the extracted average aggregation numbers are also in very good agreement with the quantum mechanically calculated spectra for aggregates. The latter are depicted, for oligomers consisting up to nine units, in Figure 5. In calculation of the spectra, the orientation angle was set to $\gamma = 28°$, and we adopted the coupling to a value of $J = 0.065$ eV.[44] Clearly, the trend that with decreasing aggregate size the band ratio approaches a value of 1 is reproduced. Here we note, that the spectral changes cannot be explained within a model of coupled electronic states with no vibrations included. The actual dynamics is rather complicated because we here are in the intermediate coupling limit which does not allow for a decoupling of the electronic and vibrational degrees of free-

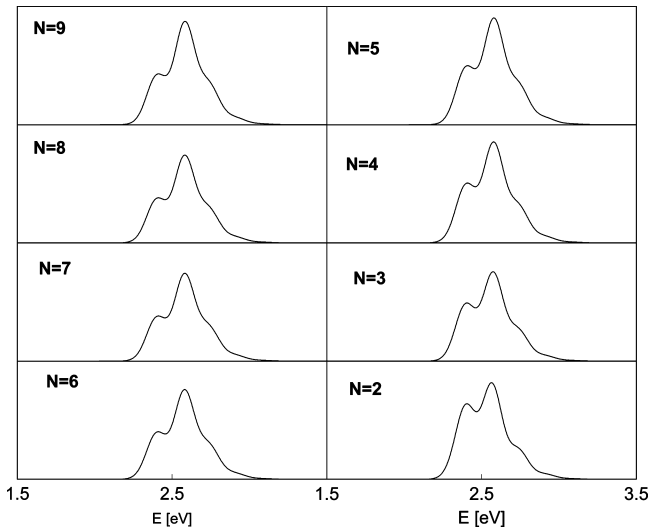

Figure 5. Calculated absorption spectra (normalized) for different aggregate sizes (N), as indicated.

dom.[55] Then, the intensity changes cannot be explained as in the weak coupling case[49] because the two appearing maxima do not correspond to vibrational transitions in the single molecule limit. Rather, they can be identified with vibrational broadened electronic transitions as can clearly be seen in the circular dichroism spectra of PBI.[22,56]

3.4. Population Dynamics in PBI Aggregates. It is interesting to address the matter of exciton or population dynamics in the (modeled) perylene bisimide aggregates. To do so, we regard a particular configuration where all transition dipole moments are arranged symmetrically in the (x, y)-plane (with an equal angle of $\gamma = 28°$ between neighboring monomer moments). The coordinate origin is fixed in the middle of the linear aggregate, so that one finds angles γ_n of the transition dipole moment of monomer (n) with values $\gamma_n = [-((N-1)/2) + (n-1)]\gamma$. For example, in the dimer ($N = 2$) the moments have angles of $-\gamma/2$ and $\gamma/2$, and, e.g., for the trimer one finds $\gamma_1 = -\gamma$, $\gamma_2 = 0$, $\gamma_3 = \gamma$. It can be shown that a calculation for this symmetric configuration yields (besides a factor of 2/3) to the same expression for the correlation function (eq 15) and thus spectra as obtained from the angular average described in section 2.2.

In what follows, we discuss the population dynamics that starts from the initial distribution which would be prepared by a white light pulse (δ-function pulse in time)

$$P_n(t=0) = \langle \vec{\epsilon}\vec{\mu}_n\psi_i | \vec{\epsilon}\vec{\mu}_n\psi_i \rangle = \frac{1}{2}[\cos(\gamma_n) + \sin(\gamma_n)]^2 \ \langle \mu_n\psi_i | \mu_n\psi_i \rangle \quad (27)$$

These populations correspond to the one prepared in the excited state configuration where monomer (n) is excited. It is important to note that here the angle γ_n enters into the initial population. In Figures 6, 7, and 8, we show the dynamics for the aggregates with $N = 5$, 6, and 7, respectively. The populations are normalized such that $\sum_n P_n(t) = 1$. The figures contain the populations $P_n(t)$ and also a curve which is obtained by an average over a time window of 50 fs. The latter exhibit the overall dynamics much clearer.

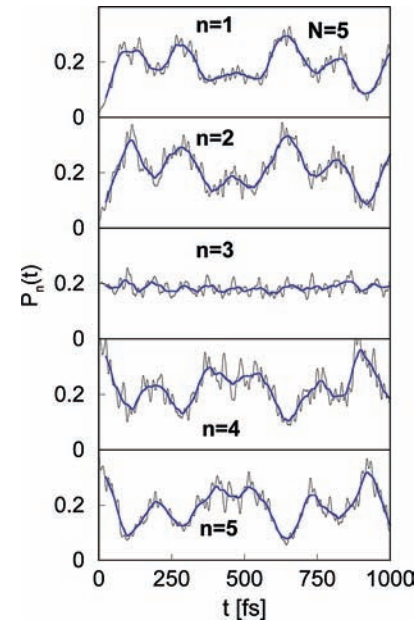

Figure 6. Population dynamics in a modeled PBI aggregate for a size of $N = 5$ units. Shown are the populations $P_n(t)$ corresponding to the configuration where monomer n is excited. The initial populations are determined by the respective transition dipole-geometry. The thick solid lines represent an average taken over a time window of 50 fs.

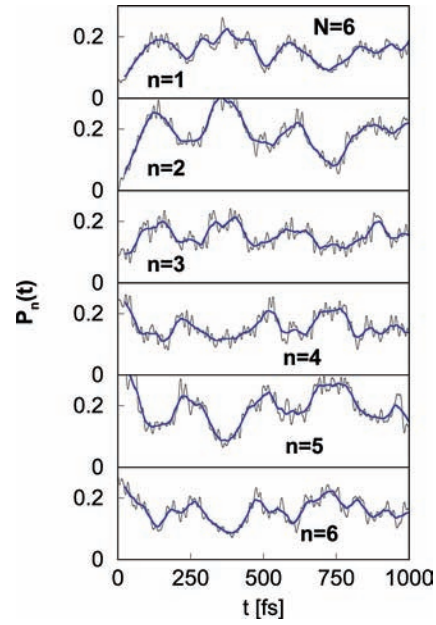

Figure 7. Same as Figure 6, but for an aggregate consisting of $N = 6$ monomers.

Starting with the $N = 5$ case, the initial distribution is such that the first two configurations ($n = 1$, 2) are almost not populated, whereas the ones with $n = 4$, 5 carry the main excitation. This changes as a function of time: the group of curves $P_1(t)$, $P_2(t)$ oscillate out of phase with the $P_4(t)$, $P_5(t)$ populations whereas the configuration where the central monomer is excited remains nearly constant. This finding suggest the picture that the excitonic excitation is localized over two or three monomer units and periodically oscillates back and forth. Of course, this is a simplified picture which ignores the vibrational wave packet dynamics in the five internal degrees of freedom.

An exciton localization on three units is encountered in the hexamer (Figure 6). There, one finds an out-of phase motion

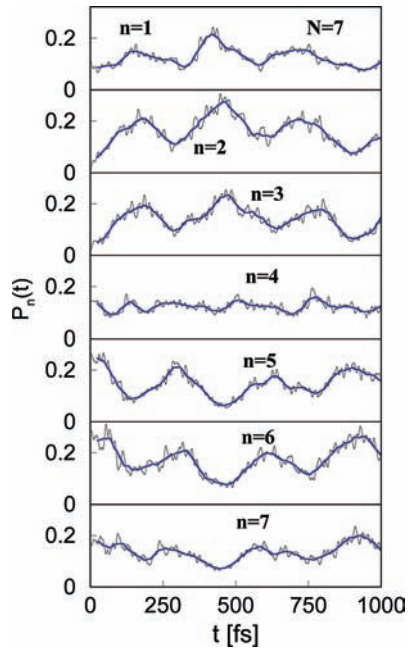

Figure 8. Same as Figure 6, but for an aggregate consisting of $N = 7$ monomers.

of the populations $P_n(t)$ with $n = 1, 2, 3$ and $n = 4, 5, 6$. The internal vibronic dynamics is even more complicated and besides the overall time variation, a more complex time behavior is encountered. In the case $N = 7$ (Figure 8) one could extract an exciton localization over three to four units because the curves with $n = 1, 2, 3$ and $n = 5, 6, 7$ oscillate out of phase and the middle monomer population shows only a smooth variation. The situation is more complicated if compared to the former ones of smaller oligomers. This is due to the initial condition at $t = 0$ which critically determines the population dynamics. If the orientation angle γ takes a value of 30°, then the initial population distribution is periodic with a periodicity of six units so that $P_7(t) = P_1(t)$. In our case ($\gamma = 28°$) this is only nearly fulfilled but, nevertheless, the initial populations at the ends of the aggregate are comparable. This illustrates that the exciton localization after δ-pulse excitation is mainly determined by the fixed geometry assumed in our calculation.

4. Summary

We theoretically investigate the absorption spectroscopy and vibronic dynamics in molecular aggregates. Oligomers consisting of up to $N = 9$ monomers are considered, where each monomer carries a vibrational degree of freedom. The time-dependent quantum calculation involves wave packet propagations in N vibrational degrees of freedom with components in N coupled electronic states. These propagations were carried out with the efficient MCTDH method.

Absorption spectra are calculated for different coupling strengths. For weak electronic coupling, the monomer spectrum splits into several vibrational bands and, with increasing aggregates size, the sublevel splitting increases. On the other hand, for a strong coupling, different electronic bands are visible which carry a vibrational structure. These bands merge with an increasing number of monomers in the aggregate. Finally, the case of intermediate coupling forbids (as always) a clear interpretation of the band/level structure.

We study the population/exciton dynamics after a localized excitation. In this way it is possible to monitor the transfer from one to the other end of the aggregate which is characterized by a specific transfer time t_{tr}. The calculations confirm the expectations that this time increases nonlinearly with the aggregated size, whereas the transfer efficiency decreases. It is seen, that the latter is smallest in the case of intermediate coupling.

Experiments have been performed on aggregates of perylene bisimides which are produced at different temperatures. Measured UV−vis spectra exhibit changes as a function of temperature. In comparing the experimental and theoretical spectra it is possible to obtain insight into the distribution of aggregate sizes at a given temperature. The here deducted average aggregate sizes are in perfect agreement with our former analysis based on the isodesmic aggregation model.[22]

Assuming a fixed geometry where the next neighbor transition dipole moments are oriented at the same angle, we showed that for oligomers up to $N = 7$, the initial population of the different excited state configurations results in an exciton localization over three to four units. This distribution, which is maintained as a function of time (for the isolated system) is determined exclusively by the transition-dipole geometry. It is worthwhile to include a coupling to a surrounding into the theoretical description. This is also possible within the MCTDH method and will be taken up in future work.

Acknowledgment. Financial support by the DFG within the Graduiertenkolleg 1221 is gratefully acknowledged. We thank Prof. W. Schenk for stimulating discussions.

References and Notes

(1) Förster, T. *Ann. Phys.* **1948**, *437*, 55.
(2) Fulton, R. L.; Gouterman, M. *J. Chem. Phys.* **1964**, *41*, 2280.
(3) Gregory, A. R.; Henneker, W. H.; Siebrand, W.; Zgierski, M. Z. *J. Chem. Phys.* **1975**, *63*, 5475.
(4) Kopainsky, B.; Hallermeier, J. K.; Kaiser, W. *Chem. Phys. Lett.* **1981**, *83*, 498.
(5) Scherer, P. O. J.; Knapp, E. W.; Fischer, S. F. *Chem. Phys. Lett.* **1984**, *106*, 6149.
(6) Kühn, O.; Renger, T.; May, V. *Chem. Phys.* **1996**, *204*, 99.
(7) Renger, T.; Voigt, J.; May, V.; Kühn, O. *J. Phys. Chem.* **1996**, *100*, 15654.
(8) Friesner, R.; Silbey, R. *J. Chem. Phys.* **1981**, *75*, 5630.
(9) Leng, W.; Würthner, F.; Kelley, A. M. *J. Phys. Chem. B* **2004**, *108*, 10284.
(10) Eisfeld, A.; Briggs, J. S. *Chem. Phys.* **2002**, *281*, 61.
(11) Eisfeld, A.; Briggs, J. S. *Chem. Phys.* **2006**, *324*, 376.
(12) Seibt, J.; Marquetand, P.; Engel, V.; Chen, Z.; Dehm, V.; Würthner, F. *Chem. Phys.* **2006**, *328*, 354.
(13) Eiermann, H.; Wagner, M. *J. Chem. Phys.* **1996**, *105*, 6713.
(14) Seibt, J.; Dehm, V.; Würthner, F.; Engel, V. *J. Chem. Phys.* **2007**, *126*, 164308.
(15) Roden, J.; Eisfeld, A.; Briggs, J. S. *Chem. Phys.* **2008**, *352*, 258.
(16) Briggs, J. S.; Herzenberg, A. *Mol. Phys.* **1971**, *21*, 865.
(17) Eisfeld, A.; Kniprath, R.; Briggs, J. S. *J. Chem. Phys.* **2007**, *126*, 104904.
(18) Philpott, M. R. *J. Chem. Phys.* **1971**, *55*, 2039.
(19) Spano, F. C. *J. Chem. Phys.* **2002**, *116*, 5877.
(20) Spano, F. C. *J. Chem. Phys.* **2005**, *122*, 234701.
(21) Chen, Z.; Stepanenko, V.; Dehm, V.; Prins, P.; Siebbeles, L.; Seibt, J.; Marquetand, P.; Engel, V.; Würthner, F. *Chem.—Eur. J.* **2007**, *13*, 436.
(22) Dehm, V.; Chen, Z.; Baumeister, U.; Prins, P.; Siebbeles, L. D. A.; Würthner, F. *Org. Lett.* **2007**, *9*, 1085.
(23) Würthner, F. *Chem. Commun.* **2004**, 1564.
(24) Wasielewski, M. R. *J. Org. Chem.* **2006**, *71*, 5051.
(25) Elemans, J. A. A. W.; Hameren, R. V.; Nolte, R. J. M.; Rowan, A. E. *Adv. Mater.* **2006**, *18*, 1251.
(26) Meyer, H.-D.; Manthe, U.; Cederbaum, L. S. *Chem. Phys. Lett.* **1990**, *165*, 73.
(27) Manthe, U.; Meyer, H.-D.; Cederbaum, L. S. *J. Chem. Phys.* **1992**, *97*, 3199.
(28) Beck, M. H.; Jäckle, A.; Worth, G. A.; Meyer, H.-D. *Phys. Rep.* **2000**, *324*, 1.
(29) Meyer, H.-D.; Worth, G. A. *Theor. Chem. Acc.* **2003**, *109*, 251.
(30) *Multidimensional Quantum Dynamics: MCTDH Theory and Applications*; Meyer, H.-D., Gatti, F., Worth, G. A., Eds.; Wiley-VCH: Weinheim, 2009.

(31) Bredas, J.-L.; Beljonne, D.; Coropceanu, V.; Cornil, J. *Chem. Rev.* **2004**, *104*, 4971.
(32) Franck, J.; Teller, E. *J. Chem. Phys.* **1938**, *6*, 861.
(33) Merrifield, R. E. *J. Chem. Phys.* **1958**, *28*, 647.
(34) Roden, J.; Schulz, G.; Eisfeld, A.; Briggs, J. S. *J. Chem. Phys.* **2009**, in press.
(35) Gordon, R. G. *Adv. Magn. Reson.* **1968**, *3*, 1.
(36) Heller, E. J. *Acc. Chem. Res.* **1981**, *14*, 368.
(37) Schinke, R. *Photodissociation Dynamics*; Cambridge University Press: Cambridge, 1993.
(38) Tannor, D. J. *Introduction to Quantum Mechanics: A Time-dependent Perspective*; University Science Books: Sausalito, CA, 2007.
(39) Engel, V.; Schinke, R.; Hennig, S.; Metiu, H. *J. Chem. Phys.* **1990**, *92*, 1.
(40) May, V.; Kühn, O. *Charge and Energy Transfer Dynamics in Molecular Systems*; Wiley-VCH: Berlin, 2000.
(41) Potma, E. O.; Wiersma, D. A. *J. Chem. Phys.* **1998**, *108*, 4894.
(42) Bednarz, M.; Malyshev, V. A.; Knoester, J. *J. Chem. Phys.* **2004**, *120*, 3827.
(43) Heijs, D. J.; Malyshev, V. A.; Knoester, J. *J. Chem. Phys.* **2005**, *123*, 144507.
(44) Fink, R.; Seibt, J.; Engel, V.; Renz, M.; Kaupp, M.; Lochbrunner, S.; Zhao, H.-M.; Pfister, J.; Würthner, F.; Engels, B. *J. Am. Chem. Soc.* **2008**, *130*, 12858.
(45) Hippius, C.; van Stokkum, I. H. M.; Zangrando, E.; Williams, R. M.; Wykes, M.; Beljonne, D.; Würthner, F. *J. Phys. Chem. C* **2008**, *112*, 14626.
(46) Worth, G. A.; Beck, M. H.; Jäckle, A.; Meyer, H.-D. *The MCTDH Package, Version 8.2*, 2000. Meyer, H.-D. *Version 8.3*, 2002; *Version 8.4*, 2007. See http://mctdh.uni-hd.de.
(47) Bacic, S.; Light, J. C. *J. Chem. Phys.* **1986**, *85*, 4594.
(48) Simpson, W. T.; Peterson, D. L. *J. Chem. Phys.* **1957**, *26*, 588.
(49) Spano, F. C. *Chem. Phys.* **2006**, *325*, 22.
(50) Clark, J.; Silva, C.; Friend, R. H.; Spano, F. C. *Phys. Rev. Lett.* **2007**, *98*, 206406.
(51) Clark, J.; Chang, J.-F.; Spano, F. C.; Friend, R. H.; Silva, C. *Appl. Phys. Lett.* **2009**, *94*, 163306.
(52) Hsu, C.-P. *Acc. Chem. Res.* **2009**, *42*, 509.
(53) Seibt, J.; Engel, V. *Chem. Phys.* **2007**, *338*, 143.
(54) Martin, R. B. *Chem. Rev.* **1996**, *96*, 3043.
(55) Eisfeld, A.; Seibt, J.; Engel, V. *Chem. Phys. Lett.* **2008**, *467*, 186.
(56) Seibt, J.; Dehm, V.; Würthner, F.; Engel, V. *J. Chem. Phys.* **2008**, *128*, 204303.

JP904892V